Absorption of Mercury in Gold Films and Its Further Desorption: Quantitative Morphological Study of the Surface Patterns

Marcin Fiałkowski,*,† Patrycja Grzeszczak,† Robert Nowakowski,† and Robert Hołyst†,‡

Institute of Physical Chemistry, Polish Academy of Sciences, Kasprzaka 44/52, 01-224 Warsaw, Poland, and Department of Mathematics and Natural Sciences - College of Science, Cardinal Stefan Wyszyński University, Dewajtis 5, 01-815 Warsaw, Poland

Received: August 26, 2003; In Final Form: February 12, 2004

A thin film of Au exposed to mercury vapor disrupts forming separated domains of AuHg amalgam. After evaporation of Hg at high temperature Au islands are formed and the domain pattern changes. A detailed quantitative morphological analysis and comparison of two types of surface patterns before and after the evaporation of Hg is performed. We have found that during the evaporation of Hg at high temperature the islands decrease their sizes and their shapes become more circular. The domain pattern formed by the amalgam domains is found to be characterized by one length scale. After the removal of mercury the characteristic length scale vanishes and the structure function takes the shape typical for the random droplet morphologies.

1. Introduction

Mercury and volatile mercury are well-known contaminants and therefore various experimental methods have been used to detect and remove Hg from the environment. Gold is well-known to be a strong absorber of mercury and that is why it is very often used as a sensitive material to detect it. In principle gold can also be used as a passive collector of the mercury with the easy release of the mercury load by the heating/Hg evaporation mechanism. There are many techniques for the detection of mercury in the gold films. Gaseous mercury interacts with the gold film forming an amalgam. It results in the increase of the film mass. If the film is subjected to the oscillations, then the absorption of Hg decreases the frequency of such oscillations.[1] Another method is based on desorption of the mercury from the taken sample, its further adsorption on the gold film and finally desorption to the gold−mercury vapor analyzer. It is called a field screening method and is used for the detection of Hg in the soil sample analysis.[2] There are a number of electrochemical methods used to analyze even the traces of Hg in water.[3−5] In this method mercury is electrodeposited on a gold electrode that is either stationary[5] or rotating.[3,4] The films can be analyzed by, e.g., surface plasmon resonance spectroscopy,[6] X-ray photoelectron spectroscopy,[5] scanning Auger microscopy, or SEM.[7] Despite the numerous studies of the absorption of mercury on gold films, the process is far from being understood. In typical experiments the gold films are exposed to mercury for a few minutes only, which results in the surface absorption of the latter. However, when the exposition time is longer than a few hours, the gold films undergo irreversible changes due to the formation of AuHg amalgam in the bulk.[7−10] Usually, the film disrupts and islands of the amalgam of various sizes and shapes are formed. The observed drastic changes in the film topography strongly depend on the gas phase composition, which influences the kinetics of the amalgam formation. This process was carefully examined using combined AFM and X-ray diffraction for amalgams of gold[8,9] and silver.[10] It has been observed that continuous thin gold or silver films are transformed into separated clusters as the result of interaction with mercury vapor (for several hours) under vacuum conditions. The surface pattern can be very well analyzed by the STM or AFM methods.[8,11] However, the image analysis of the two-dimensional patterns obtained in the STM or AFM experiments is usually qualitative or even only descriptive.[12,13] It is a purpose of this paper to present a full morphological analysis of the surface pattern formed in the absorption of mercury in thin gold films. The patterns before and after evaporation of Hg are compared. The pattern consists of islands of different shapes and sizes. Here we give the distributions of their area and circumferences, giving in this way the quantitative morphological analysis of the pattern obtained in the AFM experiment. The analysis is based on the methods known in the study of the cellular structures. 2D cellular structures are known in many areas of science.[14] Whether we consider bee's honeycomb, soap foam (or froth),[15−17] defects condensation of charge density waves,[18] territory of fire ants,[19] administrative divisions,[20,21] superclusters of galaxies (large scale structure of the universe),[22] 2D sections of polycrystalline materials, chemical patterns on surfaces, and crack structure in ceramics,[23] we find characteristic morphological patterns. Such patterns subjected to the detailed quantitative morphological analysis, as in the case of a 2D transition in magnetic systems,[24] or kinetic roughening of the etched Si[25] can give information about the mechanisms of their formation and characteristics of the distribution of the domains. This in turn may be useful in the characterization of the given material by its two-dimensional surface pattern. The rest of the paper is organized as follows: In the next section the experimental part of our work is described. In section 3 the morphological analysis and comparison of the two types of surface patterns are presented. Summary of the results and conclusions are given in the section 4.

2. Experimental Section

The experimental procedure was the same as described in detail previously.[9,10] Gold film was deposited on glass plates (1 cm^2, Menzel Glaser, Germany) by Au evaporation from a

† Polish Academy of Sciences.
‡ Cardinal Stefan Wyszyński University.

10.1021/jp0365413 CCC: $27.50 © 2004 American Chemical Society
Published on Web 03/27/2004

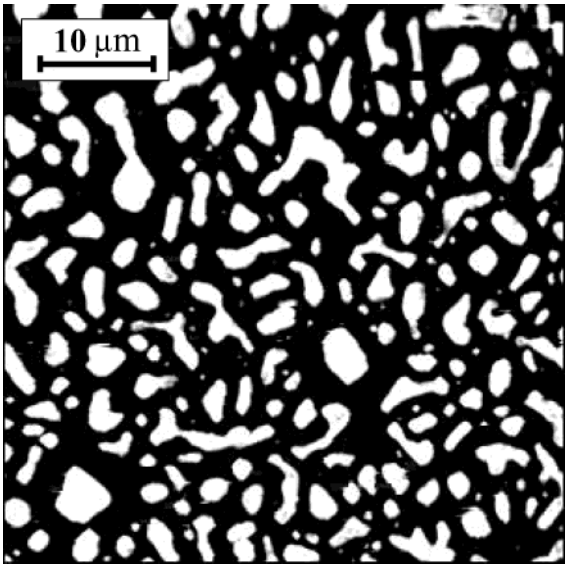

Figure 1. Structure formed in the absorption of mercury in thin gold films obtained using an AFM microscope (the height of amalgam clusters varies between 300 and 800 nm). The film was exposed to the mercury vapor for about 15 h. The white color corresponds to the domains of the AuHg amalgam.

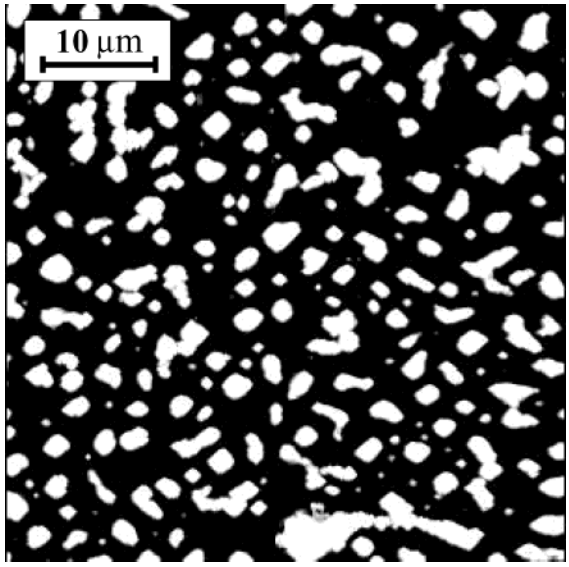

Figure 2. Domains of gold obtained after heating the AuHg alloy formed on the glass substrate (the height of gold clusters varies between 200 and 700 nm). The image was obtained using an AFM microscope. The white color corresponds to the Au islands.

tungsten heater under UHV conditions (base pressure below 10^{-7} Pa). The temperature of the support during the evaporation was maintained at 78 K. Immediately after deposition, the films (of average thickness about 40 nm) were sintered under UHV conditions at 370 K for a period of 15 min. Then the chamber was slowly cooled to room temperature. After the preparation of thin Au films the samples were exposed to Hg vapor under static vacuum conditions, having the residual gas pressure of the order of 10^{-4} Pa. At room temperature the equilibrium Hg vapor pressure reaches 0.24 Pa. The exposition time was about 15 h. Next, the samples were removed from the vacuum system, to perform the AFM investigations. The amalgamation of gold film in vacuum conditions leads to the formation of well isolated islands of amalgam on a glass substrate. The discontinuity of the obtained film was confirmed by AFM observation and by a drastic change of the electric resistance of the film measured in situ during amalgamation.[9,10] The example of a surface pattern of an amalgam film is shown in Figure 1. Next, the alloys were again moved to the vacuum chamber and heated at temperatures of 500 K for 2 h. Finally, the samples were cooled to room temperature and removed to ambient conditions. AFM investigations were then performed on the gold film after amalgam decomposition (as confirmed by XRD measurements[9]). In Figure 2 a typical system of the Au islands obtained after the heating of the gold amalgam is shown.

AFM measurements were performed using a commercial SPM system Discoverer Topometrix. The topography of the samples after amalgamation and after amalgam decomposition were studied in contact and constant force modes. Standard Si_3N_4 tips were used. All investigations were performed under ambient atmosphere. Then the results, 10 images of different places (scanning areas 50×50 μm^2) for each sample, were collected and transferred to the computer program for morphological analysis.

3. Morphological Characterization of the Surface Patterns

The digital images obtained using the AFM microscope were investigated with the help of our software[26,27] developed for two-dimensional morphological analysis. We have analyzed the morphology of the domains as well as their spatial arrangement on the substrate. The global morphological measures of the patterns such as the area fraction covered by the domains, the mean length of the domain borderline per unit area, and the average number of domains per unit area have been investigated. Both for the patterns after and before the evaporation of Hg the results were averaged over 10 images, taken in different places of the sample. The total number of the domains analyzed was $N = 2237$ for the amalgam and $N = 1927$ for the Au surface pattern.

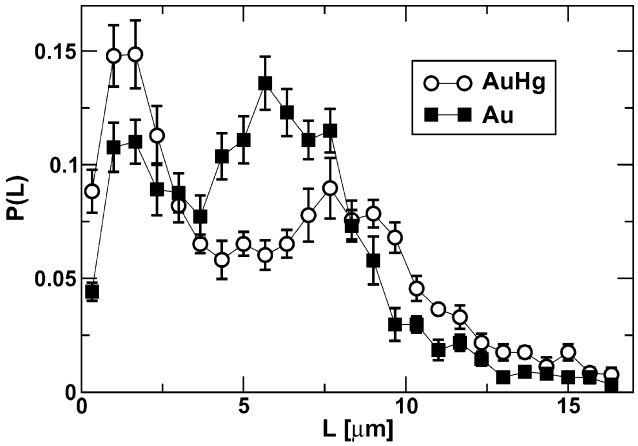

Figure 3. Distributions of the domain circumferences, L, for the AuHg (open circles) and the Au domains (squares).

3.1. Domain Sizes and Shapes. In Figure 3 the distributions $P(L)$ of the domain circumferences, L, for the patterns before and after the mercury evaporation are shown. The data are collected into 25 bins of equal size $\Delta L = 0.67$ μm. The positions of the first and the second peak are, respectively, 1.4 and 7.3 μm. After the Hg evaporation the position of the first peak remains unchanged whereas the position of the second peak is shifted to about 5.9 μm.

In Figure 4 the distributions $P(A)$ of the domain areas, A, for the patterns before and after the removal of mercury are plotted in a semilogarithmic scale. The data are grouped into 23 bins of equal size $\Delta A = 0.4$ μm^2. For the AuHg domains we have

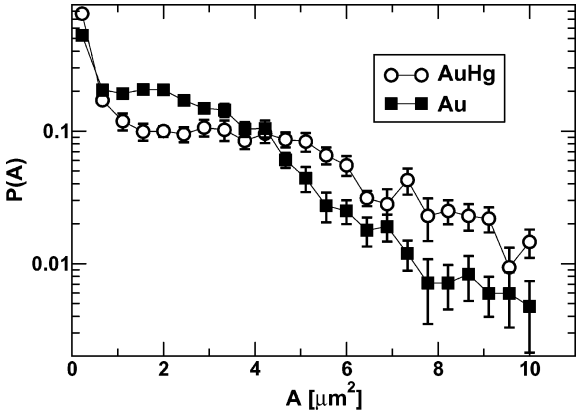

Figure 4. Distributions of the domain areas, A, for the AuHg (open circles) and the Au domains (squares).

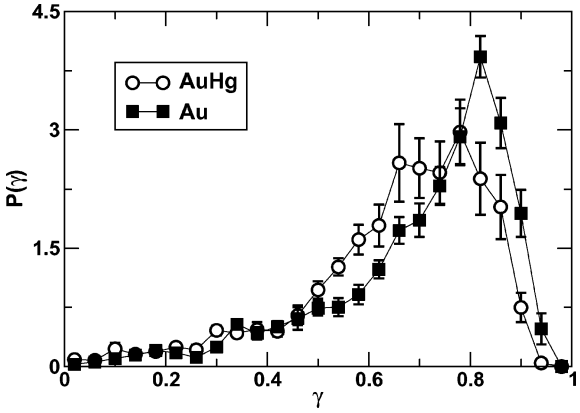

Figure 5. Distribution of the compactness parameter $\gamma = 4\pi A/L^2$ for the AuHg (open circles) and the Au domains (squares).

a peak corresponding to small domains with areas $A < 1\ \mu m^2$ and a broad plateau ranging from 1 to about 5 μm^2. After the evaporation of mercury we observe the decrease of the relative number of small domains and the function $P(A)$ exhibits a flat maximum located at about 1.9 μm^2.

To quantify the shapes of the domains, the compactness parameter γ was used. It is calculated as the following function of the domain area and its circumference:

$$\gamma = \frac{4\pi A}{L^2} \tag{1}$$

The parameter γ measures the deviation of the shape of a domain from a circle (disk). For a circle we have $\gamma = 1$, for a very elongated domain the compactness parameter tends to zero. The quantity γ given by eq 1 is a two-dimensional counterpart of the droplet compactness parameter used to characterize droplet morphology in polymer blends.[28] In Figure 5 the distributions $P(\gamma)$ for the patterns before and after the evaporation of mercury are plotted. The data are collected into 25 bins of equal size $\Delta\gamma = 0.04$. From the positions of the peaks we conclude that the removal of Hg makes the domain shapes more circular. The average value of the parameter γ for the AuHg and Au domains is 0.654 ± 0.036 and 0.703 ± 0.035, respectively.

The changes of domain shapes indicate that during the heating the amalgam islands exhibit liquid properties. They are able to decrease their contact line with the substrate reducing surface energy. From the distributions $P(L)$ and $P(A)$ we find that the bigger domains are more likely to reduce their sizes. The small domains (with the areas $A < 1\ \mu m^2$) before and after the

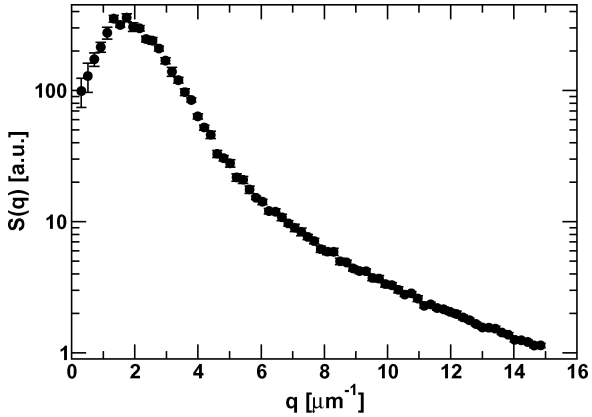

Figure 6. Structure function for the system of the AuHg domains. The shape of the function $S(q)$ obtained with a single maximum indicates that the system is characterized by one length scale L_{char}. The position of the peak corresponds to $L_{char} = 4.2\ \mu m$.

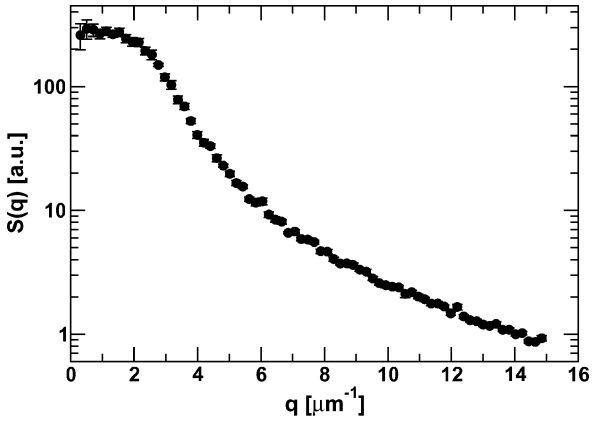

Figure 7. Structure function for the system of the Au islands obtained after the evaporation of mercury.

evaporation of Hg constitute about 94% and 73% of the total number domains, respectively (but about 5% of the total domain area in both cases). The small domains observed after the removal of mercury could be also attributed to the migration of droplets, which can merge together into bigger ones or coalesce.

3.2. Spatial Arrangement of the Domains. We have investigated spatial structure of the patterns in terms of the structure function, $S(q)$, the distribution of the distances between the domains, and the void probability function.

The structure function is calculated as

$$S(q) = \left\langle \frac{1}{L^3} \sum_r \sum_{r'} e^{iqr} \phi(r + r') \phi(r') \right\rangle \tag{2}$$

where $\phi(r)$ denotes here the domain coverage field defined as follows: If the point r belongs to the area occupied by any domain $\phi(r) = 1$, otherwise $\phi(r) = -1$. In Figures 6 and 7 the functions $S(q)$ for the patterns before and after the evaporation of mercury are shown, respectively. As we see in Figure 6, the structure function for the AuHg domains possesses characteristic maximum. This follows that the system is characterized by one length scale $L_{char} = 2\pi/q_{max}$, where q_{max} is the location of the maximum of $S(q)$. The location of the peak corresponds to $L_{char} = 4.2\ \mu m$. Note that the function $S(q)$ with a single maximum characterizes bicontinuos surface patterns formed in the processes of spinodal dewetting. This fact suggests that the disruption of the Au film exposed in mercury vapors and the spinodal dewetting might be ruled by a similar mechanism. After

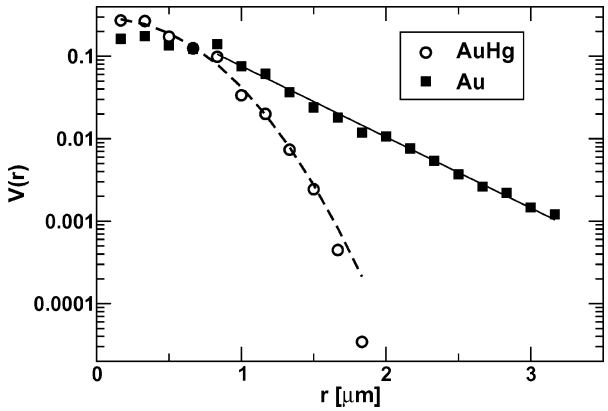

Figure 8. Void probability function, $V(r)$, calculated for the amalgam domains (open circles) and Au domains (squares). The dashed line is the least-squares fit of the stretched exponential function (see the text) to the data points. The solid line represents the least-squares fit of the exponential function for $r > 0.8$ μm.

the removal of mercury the shape of $S(q)$ changes (Figure 7). It decreases monotonically and does not exhibit the maximum. This means that the domain pattern is not described by one length scale. The shape of the structure function shown in Figure 7 is characteristic for surface patterns composed of randomly distributed domains.

The spatial distribution of the domains has also been characterized by the void probability function, $V(r)$. This function expresses the probability that a disk of radius r with a center randomly selected in the area not covered by domains does not overlap any domain. We adopt here the concept of the void distribution function from the theory of spatial point processes,[29] which is a very sensitive tool for the discrimination of different point patterns. In Figure 8 the functions $V(r)$ calculated for the AuHg and Au domain patterns are shown. As seen, for the AuHg domains a fast decay of $V(r)$ with growing r is observed. The shape of $V(r)$ is fairly well fitted by the stretched exponential function, $V(r) \sim \exp(-\alpha x^{\beta})$, where α and β are some parameters. The least-squares fit to the data points yields $\alpha = 1.93$ and $\beta = 2.17$. Interestingly, for the two-dimensional point patterns generated by the homogeneous Poisson process (HPP), $V(r)$ is given[29] by the formula $V_{HPP}(r) \sim \exp(-\rho\pi r^2)$, with ρ being the mean density of points on the plane. Because the exponent $\beta = 2.17$ does not differ much from the value of 2, we believe that some features of the amalgam domain pattern can be modeled in terms of the HPP. The density ρ_{HPP} of the HPP corresponding to the void probability obtained for the AuHg domains is $\rho_{HPP} = \alpha/\pi = 0.61$ μm^{-2}. From Figure 8 we see also that the void probability functions for the pattern before and after the evaporation of mercury differs significantly. $V(r)$ for the Au domains decays much slower and, for $r > 0.8$ μm, is well described by the exponential function.

We have also investigated distances between the domains using distribution function $D(r)$ calculated in the following way: For a point located at the border of the domain one finds the nearest point located in other domain. Denote the distance between these two points by r_{min}. The function $D(r)$ is the probability that r_{min} for a random point located at the border of the domain is equal to r. In Figure 9 the functions $D(r)$ for the patterns before and after the evaporation of mercury are plotted. As seen, both the functions have similar shapes but after the removal of Hg the maximum is shifted by $\Delta r \approx 0.5$ μm. The average distance between the domains before and after the evaporation of Hg is 1.05 ± 0.49 and 1.35 ± 0.57 μm, respectively.

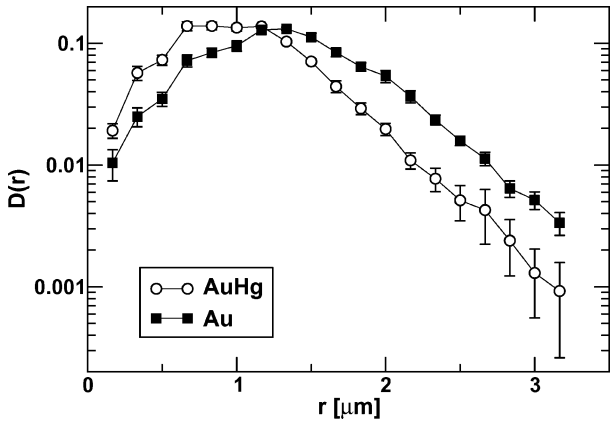

Figure 9. Distribution $D(r)$ of the distances between the domains in the AuHg amalgam (open circles) and Au (squares). The average distance between the AuHg and Au domains is 0.8 and 1.25 μm, respectively.

TABLE 1: Global Morphological Measures of the Surface Patterns before (AuHg) and after the Evaporation of Mercury (Au): the Fraction of the Area Occupied by the Domains (*a*), the Average Length of the Domain Border Line Per Unit Area (*l*), and the Average Number of Domains Per Unit Area (*n*)

	a	l (μm^{-1})	n (μm^{-2})
AuHg	0.3179 ± 0.0096	0.702 ± 0.029	0.110 ± 0.028
Au	0.197 ± 0.039	0.495 ± 0.090	0.0819 ± 0.0024

3.3. Global Morphological Measures. We have also analyzed global morphological measures of the patterns: the fraction of the area covered by the domains, a, the mean length of the domain borderline per unit area, l, and the average number of domains per unit area, n. The results are collected in Table 1. We see that after the removal of Hg a is reduced by about 38%, l decreases by 30%, and n reduces by about 25%.

4. Conclusions

In the present paper we have performed a detailed quantitative morphological analysis and comparison of two types of surface patterns obtained using the AFM technique. The first pattern was the system of the AuHg domains formed in the process of absorption of mercury in thin gold film. The second pattern was the Au domains obtained from the AuHg alloy after evaporation of mercury. We have analyzed the morphology of the domains as well as their spatial arrangement on the substrate. The global morphological measures of the patterns (the area fraction covered by the domains, the mean length of the domain borderline per unit area, and the average number of domains per unit area) have also been investigated.

The morphology of the domains has been quantified in terms of the distributions of domain areas and domain circumferences, and the distribution of the domain compactness parameter γ. The structure of the patterns and spatial arrangement of the domains have been characterized by the structure function, the distribution of the distances between the domains, and the void probability function.

The morphological analysis has shown that there are clear differences between the patterns before and after evaporation of mercury from the amalgam. The most pronounced change concerns the spatial arrangement of the domains on the substrate. The analysis of the structure factor has revealed that the domain pattern formed by the AuHg amalgam is characterized by one length scale. After the removal of mercury the characteristic

length scale vanishes and the structure function takes the shape typical for the random droplet morphologies.

We have also found that during the evaporation of mercury the domains shrink and their shapes become more circular. The changes in domain shapes and in their spatial distribution indicate that, while heating, the amalgam islands behave like a liquid, being able to migrate on the substrate and reduce their surface energy. The decrease of the number of small domains observed after the removal of mercury could be also attributed to the migration of droplets, which can merge together or coalesce.

To end, note that the morphological analysis carried out in this work provides us with a hint about possible mechanism of disruption of Au film exposed to mercury vapors. Namely, the absorption of mercury in gold films leads to the surface patterns characterized by a single length scale, which resembles bicontinuous structures formed in spinodal dewetting phenomena. Further studies are needed to check whether these two processes are governed by a similar mechanism.

Acknowledgment. This work has been supported by the KBN under Grant No. 2P03B00923 (2002-2005) and 5P03B01121 (2001-2004). We are very grateful to Prof. R. Duś for many interesting discussions and constant encouragement. M.F. acknowledges financial support from the NATO Science Fellowship.

References and Notes

(1) Caron, J. J.; Haskell, R. B.; Benoit, P.; Vetelino, J. F. *IEEE Trans. on Ultrasonics Ferroelectrics and Frequency Control* **1998**, *45*, 1393.
(2) Easterling, D. F.; Hovanitz, E. S. *Anal. Lett*. **2000**, *33*, 1665.
(3) Bonfil, Y.; Brand, M.; Kirowa-Eisner, E. *Anal. Chim. Acta* **2000**, *424*, 65.
(4) Riso, R. D.; Waeles, M.; Monbet, P.; Chaumery, C. J. *Anal. Chim. Acta* **2000**, *410*, 97.
(5) Watson, C. M.; Dwyer, D. J.; Andle, J. C.; Bruce, A. E.; Bruce, M. R. M. *Anal. Chem.* **1999**, *71*, 3181.
(6) Morrison, T.; Szulczewski, G. *Langmuir* **2002**, *18*, 5823.
(7) Battistoni, C.; Bemporad, E.; Galdikas, A.; Kaciulis, S.; Mattogno, G.; Mickevicius, S.; Olevano, V. *Appl. Surf. Sci.* **1996**, *103*, 107.
(8) Nowakowski, R.; Kobiela, T.; Wolfram, Z.; Duś, R. *Appl. Surf. Sci*. **1997**, *115*, 217.
(9) Kobiela, T.; Nowakowski, B.; Duś, R. *Appl. Surf. Sci*. **2003**, *206*, 78.
(10) Nowakowski, R.; Pielaszek, J.; Duś, R. *Appl. Surf. Sci*. **2002**, *199*, 40.
(11) Yang, X. M.; Tomani, K.; Naghara, L. A.; Hashimoto, K.; Wei, Y.; Fujishima, A. *Surf. Sci.* **1994**, *319*, L17; *Chem. Lett.* **1994**, *11*, 2059; *Surf. Sci*. **1995**, *324*, L363.
(12) Koslowski, B.; Notz, R.; Ziemann, P. *Surf. Sci*. **2002**, *496*, 153.
(13) Gimeno, Y.; Creus, A. H.; Carro, P.; Gonzalez, S.; Salvarezza, R. C.; Arvia, A. J. *J. Phys. Chem. B* **2002**, *106*, 4232.
(14) Weaire, D.; Rivier, N. *Contemp. Phys*. **1984**, *25*, 59.
(15) Stavans, J.; Glazier, J. A. *Phys. Rev. Lett*. **1989**, *62*, 1318.
(16) Hamsy, A.; Paredes, R.; Sonneville-Aubrun, O.; Cabane, B.; Botet, R. *Phys. Rev. Lett.* **1999**, *82*, 3368.
(17) Kader, A. A.; Earnshaw, J. C. *Phys. Rev. Lett*. **1999**, *82*, 2610.
(18) Weitering, H. H.; Carpinelli, J. M.; Melechko, A. P.; Zhang, J. D.; Bartkowiak, M.; Plummer, E. W. *Science* **1999**, *285*, 2107.
(19) Adams, E. S. *Ecology* **1998**, *79*, 1125.
(20) Caër, G. L.; Delannay, R. *J. Phys. I Fr.* **1993**, *3*, 1777.
(21) Glass, L.; Tobler, W. R. *Nature* **1971**, *233*, 67.
(22) Coles, P. *Nature* **1990**, *346*, 446.
(23) Korneta, W.; Mendiratta, S. K.; Menteiro, J. *Phys. Rev. E* **1998**, *57*, 3142.
(24) Fiałkowski, M.; Hołyst, R. *Phys. Rev. E* **2002**, *66*, 046121.
(25) Dotto, M. E. R.; Kleinke, M. U. *Physica A* **2001**, *295*, 149.
(26) Aksimentiev, A.; Fiałkowski, M.; Hołyst, R. *Adv. Chem. Phys*. **2002**, *121*, 141.
(27) Free software for 2D and 3D morphological analysis is available on www.ichf.edu.pl/morph.html.
(28) Tanaka, H.; Hayashi, T.; Nishi, T. *J. Appl. Phys*. **1986**, *59*, 3627.
(29) Stoyan, D.; Kendall, W. S.; Mecke, J. *Stochastic Geometry and its Applications*, 2nd ed.; John Wiley & Sons: Chichester, U.K., 1995.